Computational studies of positron states and annihilation parameters in semiconductors – vacancy-type defects in group-III nitrides –

S Ishibashi[1] and A Uedono[2]

[1] Nanosystem Research Institute (NRI) "RICS", National Institute of Advanced Industrial Science and Technology (AIST), Tsukuba, Ibaraki 305-8568, Japan
[2] Division of Applied Physics, Faculty of Pure and Applied Science, University of Tsukuba, Tsukuba, Ibaraki 305-8573, Japan

E-mail: shoji.ishibashi@aist.go.jp

Abstract. We have computationally studied positron sates and annihilation parameters in semiconductors, especially in group-III nitrides. A random alloy system $In_{0.5}Ga_{0.5}N$ was model with the special-quasirandom-structure scheme and distributions of annihilation parameters for cation monovacancies and divacancies were investigated. On GaN, we calculated annihilation parameters considering spin polarization for Ga vacancies with various charge sate and demonstrated how the positron annihilation technique is useful to study defect-induced or mediated magnetism in dilute magnetic semiconductors. We also made calculations based on the two-component density functional theory and compared their results with those obtained by the conventional scheme.

1. Introduction

Group-III nitrides are important and promising materials for various applications such as optoelectronics etc. Their properties and functions can be controlled by forming alloys and/or multilayer structures. For group-III nitride based devices, often, defects such as vacancies and dislocations play a critical role in their performances. The positron annihilation technique is known as a powerful tool to study (vacancy-type) defects in various solids including semiconductors [1,2]. We have been applying the positron annihilation technique in characterizing defects in group-III nitrides [3-5]. In this paper, we would like to report our recent progress on the computational side.

Alloys of group-III nitrides such as (Al,Ga)N and (In,Ga)N are frequently used in actual devices. It is thought that two kinds of cations are randomly distributed in these systems. To model atomic arrangements in (In,Ga)N as a random alloy, we utilized the special-quasirandom-structure (SQS) approach [6,7] and calculated positron states and annihilation parameters in bulk $In_{0.5}Ga_{0.5}N$, $In_{0.5}Ga_{0.5}N$/GaN and V_{cation} therein [5]. In the following, results for cation-nitrogen divacancies are reported.

Diluted magnetic semiconductors have been attracting much attention. Although group-III nitrides themselves are nonmagnetic *sp* systems, they can be modified to be magnetic. Gd-doped GaN is an example. On this system, Dhar *et al.* observed a large magnetic moment of 4000 μ_B per Gd atom [8]. Dev *et al.* investigated cation-vacancy induced magnetism in GaN and BN by means of electronic structure calculations [9]. Their results suggest the existence of defect-induced or mediated collective

Content from this work may be used under the terms of the Creative Commons Attribution 3.0 licence. Any further distribution of this work must maintain attribution to the author(s) and the title of the work, journal citation and DOI.
Published under licence by IOP Publishing Ltd

magnetism. Gohda and Oshiyama found that V_{Ga}s and Gd atoms are ferromagnetically-coupled and that V_{Ga}s contribute significantly to the large magnetic moment [10]. Here, we made spin-polarized calculations and obtained magnetic Doppler broadening spectra for V_{Ga}^{0}, V_{Ga}^{-1} and V_{Ga}^{-2} in GaN. To illustrate the uniqueness of the positron annihilation technique in studying vacancy assisted ferromagnetism, we calculated magnetic Compton scattering spectra also and made a comparison.

The density of positron delocalized in the bulk can be regarded as vanishingly small. For such a case, it is a reasonable assumption that positrons do not affect the electronic structure and the atomic arrangement. In the computational procedure, the electronic structure is first obtained and, with clamping it, the positron state is then calculated. In the following, we describe this procedure as the conventional scheme. As for a positron trapped at a defect, its density is finite. The electronic structure and the atomic arrangement should be affected by the trapped positron. To deal with such a case, the two-component density functional theory (TC-DFT) scheme [11,12] is appropriate. Nevertheless, the conventional scheme is frequently applied even for trapped positrons. One reason is that the TC-DFT scheme requires much more computational time than the conventional scheme. So far, we also applied the conventional scheme to calculate positron states trapped at various vacancy-type defects in group-III nitrides. To evaluate their accuracies, we have made calculations for divacancies in group-III nitrides and several other semiconductors by means of the TC-DFT.

2. Computational details

All the calculations in the present paper have been performed with our computational code QMAS (Quantum MAterials Simulator) [13].

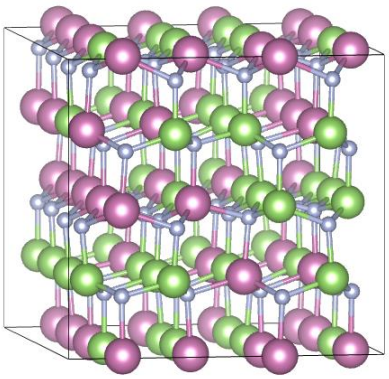

Figure 1. SQS-modelled $In_{0.5}Ga_{0.5}N$ supercell (orthorhombic cell equivalent to 4×4×2 hexagonal unit cell including 128 atoms) used in the calculation. Green, purple and small grey balls represent Ga, In and N atoms, respectively.

2.1. Structural modelling

To calculate positron states and annihilation parameters in group-III nitride systems containing defects or in alloys, we used orthorhombic supercells which are equivalent to 4×4×2 hexagonal unit cells of the wurzite structure. For cubic semiconductors, we used 2×2×2 and 3×3×3 supercells. For $In_{0.5}Ga_{0.5}N$, in which two kinds of cations are randomly distributed, we used the special-quasirandom-structure (SQS) approach [6,7]. This is a method to provide realistic structural modeling for random alloys using periodic supercells. With this method, two kinds of atoms *A* and *B* are arranged so that pair-correlation functions become as close to those for an infinite random alloy as possible. Practically, an atomic arrangement, which gives the lowest Warren-Cowley parameter for several neighboring shells, is chosen. The Warren-Cowley parameter for the *j*-th nearest neighbor shell is expressed as

$$\alpha_j = 1 - \frac{P_B(j)}{x_B}, \tag{1}$$

where $P_B(j)$ is the probability of finding a *B* atom on the *j*-th nearest neighbor shell about an *A* atom as the origin. In the present study, shells up to the 7-th are taken into account and the following quantity should be minimized:

$$T = \sum_{j=1}^{7} \alpha_j^2 . \tag{2}$$

Although the supercell dimensions are also optimized in the original SQS approach, we fixed them in the present work. In figure 1, the SQS-modelled $In_{0.5}Ga_{0.5}N$ supercell is shown. From this structure, an initial structure for a defect system was prepared by removing (an) atom(s).

2.2. Electronic structure calculation

Electronic structures were calculated based on the DFT within the generalized gradient approximation using the exchange-correlation functional of Perdew, Burke and Ernzerhof (PBE) [14]. Electronic wave functions are described with the plane-wave basis in the framework of the projector augmented-wave (PAW) method [15]. The PAW method is adequate to obtain the momentum density distribution of annihilation quanta accurately even in a higher momentum region [16,17]. It is also known to be more efficient than the norm-conserving pseudopotential method. The plane-wave energy cutoff and the force convergence criterion were set to be 20 Ha and 5×10^{-5} Ha/bohr, respectively, for all the calculations with the conventional scheme. As for $\boldsymbol{k}$ point sampling, only the Γ point was used except for spin-polarized calculations on the GaN supercell, where 2×2×2 $\boldsymbol{k}$ points were used.

2.3. Positron state and annihilation parameters

The positron effective potential was constructed using core electron wave functions from isolated atom calculations and valence electron wave functions described in the PAW formalism [15]. As for the positron-electron correlation potential term, we used that proposed by Boroński and Nieminen [11]. The positron wave function is also described with the plane-wave basis and optimized in the reciprocal space iteratively. With the obtained positron and electron wave functions, the momentum distribution of annihilation quanta $\rho(\mathbf{p})$ and positron lifetimes τ were calculated with the following equations:

$$\rho(\mathbf{p}) \propto \sum_j \left| \int \psi_+(\mathbf{r}) \psi_{-j}(\mathbf{r}) \sqrt{\gamma(n_-(\mathbf{r}))} \exp(-i\mathbf{p}\cdot\mathbf{r}) d\mathbf{r} \right|^2 , \tag{3}$$

$$1/\tau = \lambda = \pi r_0 c \int n_+(\mathbf{r}) n_-(\mathbf{r}) \gamma(n_-(\mathbf{r})) d\mathbf{r} , \tag{4}$$

where ψ_+, ψ_{-j} , n_+ and n_- are the positron wave function, the *j*-th electron wave function, the positron density and the electron density, respectively. r_0 represents the classical electron radius and *c* is the speed of light. γ is the enhancement factor. We used the Boroński-Nieminen enhancement factor

$$\gamma_{\mathrm{LDA}} = 1 + 1.23 r_s + 0.8295 r_s \sqrt{r_s} - 1.26 r_s^2 + 0.3286 r_s^2 \sqrt{r_s} + r_s^3/6 , \tag{5}$$

where $r_s = [3/(4\pi n_-)]^{1/3}$ is the density parameter, with a small modification to deal with semiconductors [18]. Here, in analogy with the GGA enhancement factor [19], and to be consistent with the positron-electron correlation energy, we used the expression

$$\gamma_{\mathrm{semi}} = 1 + (\gamma - 1)(1 - 1/\varepsilon_\infty) . \tag{6}$$

ε_∞ is the dielectric constant of the target system. Although it can be determined by first-principles calculations, we adopted the experimental values for convenience. In case of alloys, linearly-interpolated values were used. For reference, the expression in the original semiconductor model [18] is

$$\gamma_{\text{semi}} = 1 + \frac{(1-1/\varepsilon_\infty)r_s^3 + 10}{6}. \tag{7}$$

When we make comparisons with results obtained from TC-DFT calculations, we used

$$\gamma_{\text{semi}} = 1 + 1.23r_s + 0.9889r_s\sqrt{r_s} - 1.4820r_s^2 + 0.3956r_s^2\sqrt{r_s} + (1-1/\varepsilon_\infty)r_s^3/6, \tag{8}$$

which is compatible with that used in the TC-DFT calculations. The enhancement factor expressed in (8) corresponds to that in the vanishing n_+ limit for the TC-DFT scheme. Doppler broadening spectra were calculated by integrating equation (3)

$$J(p_z) = \iint \rho(\mathbf{p})dp_x dp_y. \tag{9}$$

If spin sign is distinguished, it is expressed as

$$J(p_z) = \iint \left(\rho_{\text{up}}(\mathbf{p}) + \rho_{\text{down}}(\mathbf{p})\right)dp_x dp_y. \tag{10}$$

From magnetic Doppler broadening measurements,

$$J_{\text{mag}}(p_z) = \iint \left(\rho_{\text{up}}(\mathbf{p}) - \rho_{\text{down}}(\mathbf{p})\right)dp_x dp_y. \tag{11}$$

Then, we can obtain

$$J_{\text{up}}(p_z) = \frac{1}{2}\left(J(p_z) + J_{\text{mag}}(p_z)\right) = \iint \rho_{\text{up}}(\mathbf{p})dp_x dp_y, \tag{12}$$

$$J_{\text{down}}(p_z) = \frac{1}{2}\left(J(p_z) - J_{\text{mag}}(p_z)\right) = \iint \rho_{\text{down}}(\mathbf{p})dp_x dp_y. \tag{13}$$

To calculate Compton scattering spectra, the following expression is used instead of equation (3):

$$\rho(\mathbf{p}) \propto \sum_j \left|\int \psi_{-j}(\mathbf{r})\exp(-i\mathbf{p}\cdot\mathbf{r})d\mathbf{r}\right|^2. \tag{14}$$

2.4. Two-component density functional (TC-DFT) scheme

According to [12], we made calculations with following steps:

(1) The electronic structure is calculated neglecting the presence of positron.
(2) The positron state is calculated with the results obtained in the (1) or (3) step.
(3) The electronic structure is calculated considering the positron state obtained in (2).
(4) Steps (2) and (3) are repeated to obtain the convergence of the electron and positron states.
(5) The atomic positrons are optimized calculating forces considering the positon effect.

Steps (1)-(5) are repeated to obtain the converged result. Because of steps (2)-(4), more computational time is required compared with the conventional method. The force convergence criterion was set to 5×10^{-5} Ha/bohr.

As for the electron-positron correlation energy and potentials, we used the expressions and interpolation scheme in [12]. Correspondingly, we used the enhancement factor evaluated by the interpolation scheme in [11,12] with a modification for semiconductors [20].

3. Results and discussion

Measured Doppler broadening spectra are often analysed through *S* and *W* parameters. As shown in figure 2, the *S* parameter is defined as the ratio of the center area to the total spectrum area while the *W* parameter is that for the higher momentum areas. Positrons trapped at a defect usually give a higher *S* value and a lower *W* value since an increase of the open volume size results in narrowing of the

spectrum. For all the calculations in the present study, S is evaluated in the momentum region between ± 0.419 a.u. while W is evaluated in the regions of ± (1.828~3.688) a.u. Plotting S and W together on a two-dimensional map is useful to identify defect species. If there is only one type of defect in the system, observed parameters S_{obs} and W_{obs} should be described with the parameters for the bulk S_b and W_b and those for the defect S_d and W_d as $S_{obs} = f_b S_b + f_d S_d$ and $W_{obs} = f_b W_b + f_d W_d$ ($f_b + f_d = 1$). The point (S_{obs}, W_{obs}) should be located on the line connecting (S_b, W_b) and (S_d, W_d) shown in figure 3(a). If there are two types of defects, denoting parameters for the second defect as $S_{d'}$ and $W_{d'}$, $S_{obs} = f_b S_b + f_d S_d + f_{d'} S_{d'}$ and $W_{obs} = f_b W_b + f_d W_d + f_{d'} W_{d'}$ ($f_b + f_d + f_{d'} = 1$). In this case, the point (S_{obs}, W_{obs}) should be located inside the triangle connecting (S_b, W_b), (S_d, W_d) and ($S_{d'}$, $W_{d'}$) shown in figure 3(b). In practical situations, the point (S_{obs}, W_{obs}) moves by, for example, annealing. In a certain case, vacancies aggregate to form vacancy clusters, while, in another case, vacancies form complexes with impurity atoms. Theoretical predictions are expected to be useful to distinguish them.

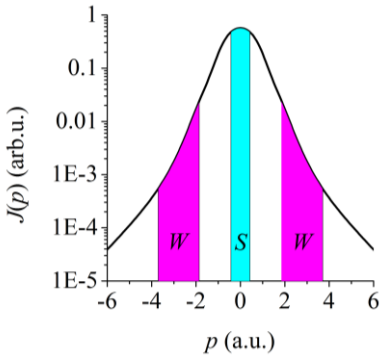

Figure 2. Definition of S and W. S and W are given as ratios of the shaded areas to the total area.

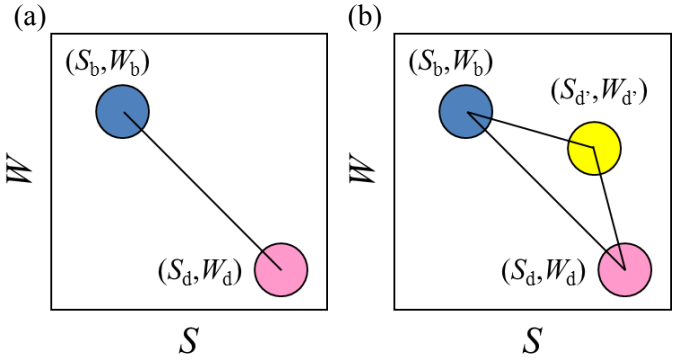

Figure 3. Schematic S–W plots for the positron annihilation from the defect-free state (S_b, W_b) and the trapped state by defects which show different (S,W) values: [(S_d, W_d) and ($S_{d'}$,$W_{d'}$)].

3.1. Divacancy in $(In_{0.5}Ga_{0.5})N$

In our previous work [5], we calculated S and W parameters for 64 types of cation vacancies in $(In_{0.5}Ga_{0.5})N$ (a supercell modelled by the SQS approach [6,7]) and found an extended distribution of S in the S–W plot. Tuomisto *et al.* also reported similar finite spreads of positron annihilation parameters (S, W and the positron lifetime) for cation monovacancies in (In,Ga)N systems [21].

In the present work, we calculated S and W parameters for 104 types of cation-nitrogen divacancies, which are randomly selected among 256 possibilities, in $(In_{0.5}Ga_{0.5})N$. The results are plotted together with those for the bulk and cation monovacancies in figure 4. As for the S parameter, significant variation has been observed and there is a finite overlap in the S–W plot between two types of defects. We also plot each S, W and the positron lifetime τ in figure 5 as a function of x_{Ga}, which represents the gallium concentration of the neighboring cation shells containing 12 sites. Although it is somewhat obscure, there seems to be positive correlation.

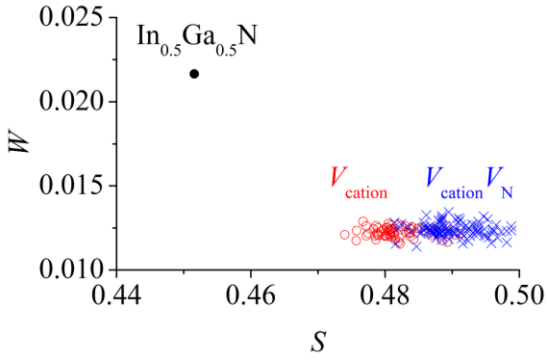

Figure 4. *S*–*W* plot for bulk $In_{0.5}Ga_{0.5}N$, cation monovacancies and cation-nitrogen divacancies.

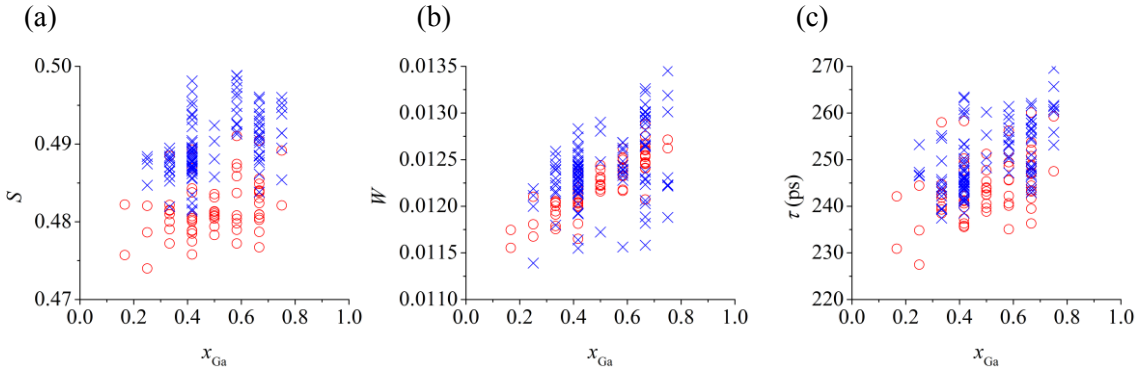

Figure 5. Positron annihilation parameters (a) *S*, (b) *W*, (c) τ for cation vacancies (○) and cation-nitrogen divacancies (×) as a function of neighbouring gallium concentration x_{Ga}.

3.2. Vacancy assisted ferromagnetism in GaN

First, spin-polarized calculations were made on the 4×4×2 supercell containing a gallium monovacancy ($Ga_{63}N_{64}$) with optimizing the atomic positions. In figure 6, obtained spin density distributions around V_{Ga}^{0}, V_{Ga}^{-1} and V_{Ga}^{-2} are shown. Dumbbell-like spin density distributions are observed. Each of them corresponds to the 2*p*-like orbital of nitrogen. The gallium vacancy is surrounded by four major dumbbells. The calculated net magnetic moment values are 3 μ_B, 2 μ_B and 1 μ_B for V_{Ga}^{0}, V_{Ga}^{-1} and V_{Ga}^{-2}, respectively.

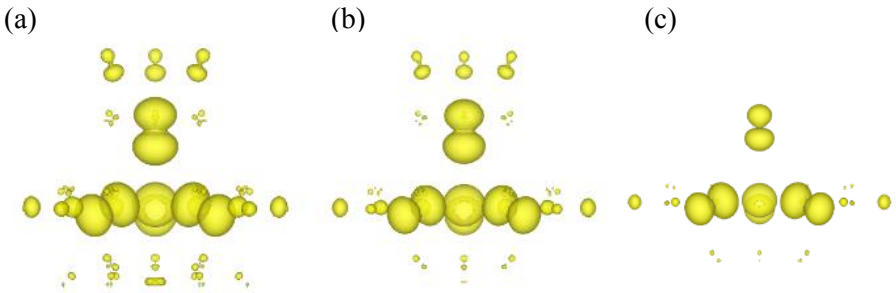

Figure 6. Spin density distribution around (a) V_{Ga}^{0}, (b) V_{Ga}^{-1} and (c) V_{Ga}^{-2}. Each dumbbell-like distribution corresponds to the 2*p*-like orbital of nitrogen. The gallium vacancy is surrounded by four major dumbbells.

Magnetic Doppler broadening and Compton scattering spectra were calculated along the $[1\bar{1}00]$ direction for three systems mentioned above. The obtained results are shown as $(\rho_{up}-\rho_{down})/(\rho_{up}+\rho_{down})$

in figure 7. It is clearly shown that the magnetic Doppler spectra are approximately 20 times enhanced than the magnetic Compton ones. This is because positrons are selectively trapped at V_{Ga}. The positron annihilation Doppler broadening technique is expected to be uniquely sensitive for vacancy-assisted ferromagnetism. It is also noted that curve intervals are more or less similar to each other reflecting the magnetic-moment difference in the graph of the Compton scattering spectra while it is not the case with the Doppler broadening spectra. It should be attributed to the positron density distribution localized at V_{Ga}. A detailed analysis is ongoing. For reference, the (S, W) values were evaluated from the spin-integrated spectra as (0.471, 0.0163), (0.474, 0.0146) and (0.474, 0.0135) for V_{Ga}^{0}, V_{Ga}^{-1} and V_{Ga}^{-2}, respectively. The S parameter is almost unchanged while the W parameter decreases slightly with the charge state varying from neutral to doubly negative.

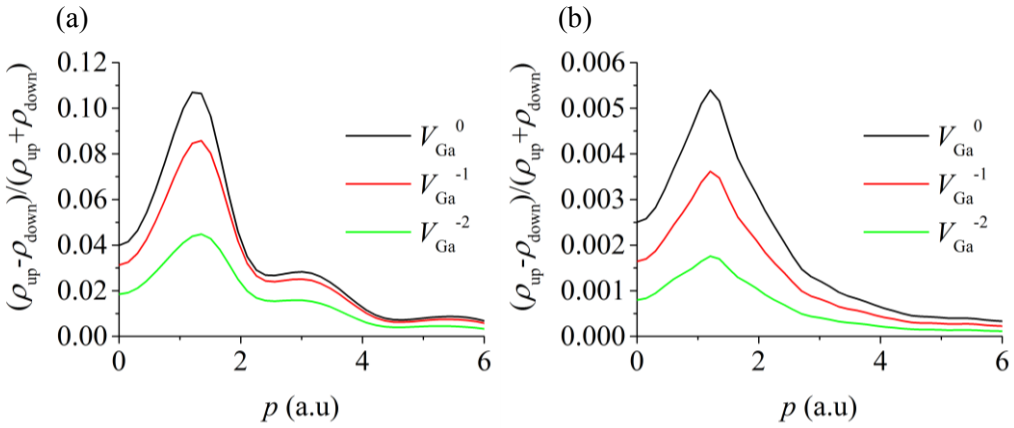

Figure 7. One-dimensional projection of spin density distribution along [1$\bar{1}$00] for V_{Ga}^{0}, V_{Ga}^{-1} and V_{Ga}^{-2}: (a) Doppler broadening and (b) Compton scattering

3.3. Two-component density functional theory scheme

First, we would like to mention our calculations for monovacancy (V) and divacancy (V_2) in Si. The calculated lifetime values are listed in table 1. It is clearly shown that there is a strong supercell-size dependence for the conventional scheme. The main reason is the difference in the atomic arrangement in the vicinity of V or V_2. The larger supercell, the larger inward relaxation is observed. This tendency and the defect structures are consistent with the previous studies [22,23]. On the other hand, for the TC-DFT scheme, the resultant lifetimes are longer than those obtained with the conventional scheme and show a much smaller supercell-size dependence. The monovacancy is surrounded by four Si atoms (1~4) showing the T_d point symmetry in the unrelaxed structure. Six distances between two of them (d_{12},d_{13},d_{14},d_{23},d_{24},d_{34}) are equivalent to each other in this case and the value is 3.84 Å. After structural relaxation, with the 2×2×2 supercell, the distance decreases to 3.67 Å (−4.4 %) for the conventional scheme while it increases to 4.00 (+4.2 %) for the TC-DFT scheme. With the 3×3×3 supercell, the point symmetry becomes D_{2d}. There are four equivalent distances (d_{13},d_{14},d_{23},d_{24}) of 3.45 Å (−10.1 %) and two distances (d_{12}, d_{34}) of 3.00 Å (−21.9 %) for the conventional scheme while four distances of 3.93 Å (+2.4 %) and two distances of 3.70 Å (−3.7 %) for the TC-DFT scheme. The presence of positron suppresses the inward relaxation around V. A similar situation is observed for V_2 as described below together with results of other semiconductors. This has been already found and reported by Saito and Oshiyama [24] although they used a different version of TC-DFT [25]. They obtained 279 ps for V and 309 ps for V_2 with the 2×2×2 supercell. Considering that they did not modify the enhancement factor with ε_∞, their values seem to be slightly overestimated. In other words, the positron effect seems to be slightly overestimated.

Table 1. Calculated positron lifetimes (in ps) for monovacancy (V) and divacancy (V_2) in Si with the conventional scheme and the TC-DFT scheme on different-sized supercells.

	Conventional		TC-DFT	
	2×2×2	3×3×3	2×2×2	3×3×3
V	232.5	222.8	267.7	268.6
V_2	282.7	247.4	314.8	315.2

Table 2. Distance between atoms neighbouring divacancy (in Å). In parentheses, relative changes from the unrelaxed values are shown (in %).

		Conventional		TC-DFT	
		cation	anion	cation	anion
C	2×2×2	2.69 (+6.7)		2.75 (+9.2)	
	3×3×3	2.65 (+5.2)		2.73 (+8.4)	
Si	2×2×2	3.62 (−5.7)		3.85 (+0.2)	
	3×3×3	3.01 (−21.7), 3.04 (−20.9), 3.55 (−7.5)		3.69 (−3.9)	
Ge	2×2×2	3.40 (−14.9)		3.50 (−12.4)	
	3×3×3	3.16 (−20.9)		3.40 (−14.8)	
3*C*-SiC	2×2×2	3.88 (+1.0)	4.15 (+8.1)	3.99 (+3.9)	4.20 (+9.5)
	3×3×3	3.08 (−0.2)	3.29 (+6.8)	3.16 (+2.6)	3.35 (+8.6)
AlN	4×4×2	3.67 (+18.0)	3.36 (+8.0)	3.76 (+20.9)	3.32 (+6.7)
GaN	4×4×2	2.98 (−6.5)	3.39 (+6.4)	3.05 (−4.4)	3.35 (+4.9)
InN	4×4×2	3.43 (−3.1)	3.56 (+0.6)	3.50 (−1.1)	3.47 (−2.1)

Thus, the conventional scheme is thought to be not very accurate at least for V and V_2 in Si, and we made calculations for divacancies in several semiconductors including group-III nitrides (C, Si, Ge, 3*C*-SiC, AlN, GaN and InN). Each anion (cation) vacancy forming a divacancy has three nearest neighbor cation (anion) atoms. For elemental semiconductors, although there is no distinction between cation and anion, there are similar 3×2 neighbor atoms. In table 2, distances between two of three atoms are listed. Except for the case of Si with the 3×3×3 cell and the conventional scheme, three distances are almost equal to each other. Correspondingly, positron annihilation parameters S, W and τ were calculated and the results are plotted in figure 8 as a function of bulk modulus. Roughly speaking, the softer material with the smaller B gives the larger difference between the results of the conventional and TC-DFT schemes. For the cubic materials, it is also confirmed that the supercell-size dependence is larger in softer materials. In figure 8(c), for Si and Ge, it looks that the conventional-scheme results with the smaller (2×2×2) cell are better than those with the larger (3×3×3) cell. As mentioned above, the inward relaxation is suppressed in the smaller cell. This is because the supercell size is too small for complete relaxation. For the TC-DFT case, the inward relaxation is suppressed by the presence of positron. The mechanism is different. The better agreement for the smaller cell is not essential.

For 3*C*-SiC, Wiktor *et al.* reported a TC-DFT lifetime of 195 ps for V_C (217 ps with the different version TC-DFT [25]) and also a value of 154 ps obtained with the conventional scheme [20]. We also made a TC-DFT calculations on for V_C in 3C-SiC and obtained a lifetime of 142 ps. Our value is quite different from the value by Wiktor *et al.* The reason is not clear yet.

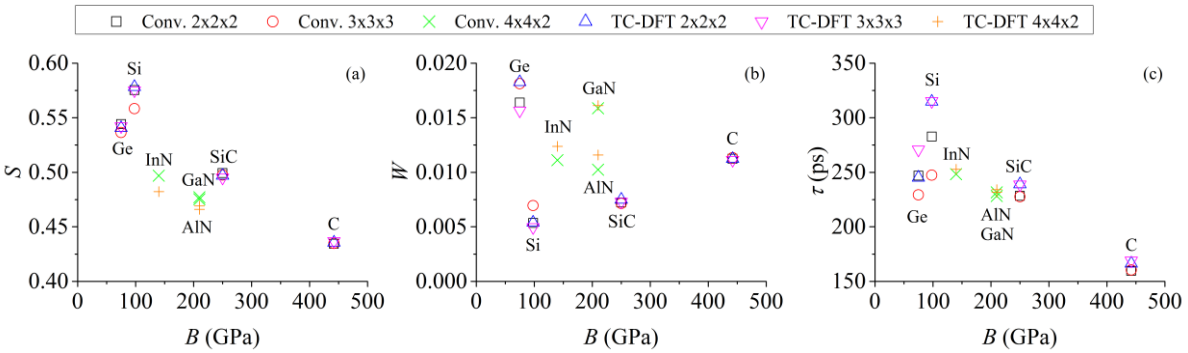

Figure 8. Positron annihilation parameters for the annihilation of positrons trapped by divacancies in various semiconductors. Calculated values of (a) S, (b) W and (c) τ are plotted as a function of bulk modulus.

As shown in figure 8, for C and SiC, the conventional-scheme results are very close to the corresponding TC-DFT ones. On the other hand, there are large deviations for the positron lifetime in Si and Ge between the two schemes. For the other cases, it depends on the situation whether or not the conventional scheme is sufficient to obtain reasonable results. For group-III nitrides, judging from the (S,W) or τ variation shown in figures 4 and 5, the conventional-scheme results can be used for our purpose identifying defect species.

4. Summary

We have made computational studies on defects in semiconductors, especially those in group-III nitrides. Variations of positron annihilation parameters S, W and τ for cation monovacancies and cation-nitrogen divacancies in $(In_{0.5}Ga_{0.5})N$ were examined utilizing the SQS approach to reproduce its random-alloy nature. Magnetic positron annihilation Doppler broadening spectra were calculated for gallium monovancancies with various charge state. The obtained results were compared with magnetic Compton scattering spectra to demonstrate the uniqueness and usefulness of the positron annihilation technique in studying vacancy-assisted ferromagnetism in diluted magnetic semiconductors. For divacancies in several semiconductors, positron annihilation parameters S, W and τ were calculated using the conventional scheme as well as using the TC-DFT scheme. The validity of the conventional scheme has been examined and discussed for various cases.

References

[1] Krause-Rehberg R and Leipner H S 1999 *Positron Annihilation in Semiconductors* (Berlin: Springer)
[2] Tuomisto F and Makkonen I 2013 *Rev. Mod. Phys.* **85** 1583
[3] Uedono A, Ishibashi S, Oshima N and Suzuki R 2013 *Jpn. J. Appl. Phys.* **52** 08JJ02
[4] Uedono A, Sumiya S, Ishibashi S, Oshima N and Suzuki R 2014 *J. Phys.: Conf. Ser.* **505** 012009
[5] Ishibashi S and Uedono A 2014 *J. Phys.: Conf. Ser.* **505** 012010
[6] Zunger A, Wei S-H, Ferreira L G and Bernard J E 1990 *Phys. Rev. Lett.* **65** 353
[7] Mäder K A and Zunger A 1995 *Phy. Rev.* B **51** 10462
[8] Dhar S, Brandt O, Ramsteiner M, Sapega V F and Ploog K H 2005 *Phys. Rev. Lett.* **94** 037205
[9] Dev P, Zue Y and Zhang P 2008 *Phys. Rev. Lett.* **100** 117204
[10] Gohda Y and Oshiyama A 2008 *Phys. Rev.* B **78** 161201(R)
[11] Boroński E and Nieminen R M 1986 *Phys. Rev.* B **34** 3820
[12] Puska M J, Seitsonen A P and Nieminen R M 1995 *Phys. Rev.* B **52** 10947
[13] http://qmas.jp
[14] Perdew J P, Burke K and Ernzerhof M 1996 *Phys. Rev. Lett.* **77** 3865

[15] Blöchl P E 1994 *Phys. Rev.* B **50** 17953
[16] Ishibashi S 2004 *Mater. Sci. Forum* **445-446** 401
[17] Makkonen I, Hakala M and Puska M J 2006 *Phys. Rev.* B **73** 035103
[18] Puska M J, Mäkinen S, Manninen M and Nieminen R M 1989 *Phys. Rev.* B **39** 7666
[19] Barbiellini B, Puska M J, Torsti T and Nieminen R M 1995 *Phys. Rev.* B **51** 7341
[20] Wiktor J, Jomard G, Torrent M and Bertolus M 2013 *Phys. Rev.* B **87** 235207 (Note that the sign of the fourth term in their equation (A9) is wrong.)
[21] Tuomisto F, Norrman V and Makkonen I 2014 *J. Phys.: Conf. Ser.* **505** 012042
[22] Puska M J, Pöykkö S, Pesola M, and Nieminen R M 1998 *Phys. Rev.* B **58** 1318
[23] Iwata J, Shiraishi K and Oshiyama A 2008 *Phys. Rev.* B **77** 115208
[24] Saito M and Oshiyama A 1996 *Phys. Rev.* B **53** 7810
[25] Gilgien L, Galli G, Gygi C and Car R 1994 *Phys. Rev. Lett.* **72** 3214